Local structure and its implications for the relaxor ferroelectric $Cd_2Nb_2O_7$

Daniel Hickox-Young,[1] Geneva Laurita,[2] Quintin N. Meier,[3] Daniel Olds,[4] Nicola A. Spaldin,[5] Michael R. Norman,[6,*] and James M. Rondinelli[1,7,†]

[1]*Department of Materials Science and Engineering, Northwestern University, Evanston, Illinois 60208, USA*
[2]*Department of Chemistry and Biochemistry, Bates College, Lewiston, Maine 04240, USA*
[3]*Université Grenoble Alpes, CEA, LITEN, 17 rue des Martyrs, 38054 Grenoble, France*
[4]*National Synchrotron Light Source II, Brookhaven National Laboratory, Upton, New York 11973, USA*
[5]*Materials Theory, ETH Zurich, Wolfgang-Pauli-Strasse 27, 8093 Zürich, Switzerland*
[6]*Materials Science Division, Argonne National Laboratory, Lemont, Illinois 60439, USA*
[7]*Northwestern-Argonne Institute of Science and Engineering (NAISE), Northwestern University, Evanston, Illinois 60208, USA*

(Received 1 July 2022; accepted 18 August 2022; published 6 September 2022)

The relaxor ferroelectric transition in $Cd_2Nb_2O_7$ is thought to be described by the unusual condensation of two Γ-centered phonon modes, Γ_4^- and Γ_5^-. However, their respective roles have proven to be ambiguous, with disagreement between *ab initio* studies, which favor Γ_4^- as the primary mode, and global crystal refinements, which point to Γ_5^- instead. Here, we resolve this issue by demonstrating from x-ray pair distribution function measurements that locally, Γ_4^- dominates, but globally, Γ_5^- dominates. This behavior is consistent with the near degeneracy of the energy surfaces associated with these two distortion modes found in our own *ab initio* simulations. Our first-principles calculations also show that these energy surfaces are almost isotropic, providing an explanation for the numerous structural transitions found in $Cd_2Nb_2O_7$, as well as its relaxor behavior. Our results point to several candidate descriptions of the local structure, some of which demonstrate two-in/two-out behavior for Nb displacements within a given Nb tetrahedron. Although this suggests the possibility of a charge analog of spin ice in $Cd_2Nb_2O_7$, our results are more consistent with a Heisenberg-like description for dipolar fluctuations rather than an Ising one. We hope this encourages future experimental investigations of the Nb and Cd dipolar fluctuations, along with their associated mode dynamics.

DOI: 10.1103/PhysRevResearch.4.033187

I. INTRODUCTION

Relaxor ferroelectrics are a fascinating class of materials [1] whose dielectric properties depend strongly on frequency, with dynamics described by a Vogel–Fulcher relation, a relation also found for the magnetic response in spin-ice materials [2–4]. They are typically chemically complex solid solutions of perovskites, with the relaxor behavior thought to be driven by the dynamics of local polar clusters. Yet the disorder inherent in these materials inhibits unambiguous interpretation of the data, leading to differing ideas about the origin of relaxor behavior. Therefore, there has been a search for stoichiometric materials that exhibit relaxor behavior that would aid in identifying intrinsic behavior and help settle this debate.

A well-known example is the valence-precise pyrochlore $Cd_2Nb_2O_7$, which undergoes a relaxor-type ferroelectric transition between 204 K and 196 K from a cubic $Fd\bar{3}m$ phase above 204 K [Fig. 1(a)] to a polar orthorhombic phase (point group *mm*2 [5]), well described as having *Ima*2 symmetry [6,7], below 196 K. The intermediate phase between 204 K and 196 K has been challenging to identify because of its limited temperature range, but is believed to have an *mmm* point group [5], implying from group-subgroup relations that it has *Imma* symmetry [8]. This is inconsistent with density functional theory (DFT) studies that find that the structural mode that defines *Imma*, Γ_5^+, is completely stable [7,9] and so should not condense.

Comparison of the *Ima*2 structure with the cubic reference using group theory identifies Γ_4^- and Γ_5^- as the dominant distortion modes describing the symmetry-lowering process [visualized in Fig. 1(b)]. Phonons calculated from first principles for the cubic phase likewise exhibit two soft phonon modes at Γ with irreducible representations (irreps) matching the Γ_4^- and Γ_5^- distortion modes present in the *Ima*2 structure. However, the exact nature of the ferroelectric phase transition, and the role of the two distortion modes, is unclear, and differing scenarios have been proposed [10].

Furthermore, DFT identifies Γ_4^- as the more unstable mode, suggesting it is the primary driving mode, although the energy difference between the two is rather small [7,9]. However, Γ_5^- displacements are found to be dominant in global structural refinements, and exhibit a classic order-parameter-like behavior as a function of temperature, as opposed to the weak temperature dependence of Γ_4^- [6]. We therefore denote the Γ_5^--dominant phase revealed by the global refinement as

*norman@anl.gov
†jrondinelli@northwestern.edu

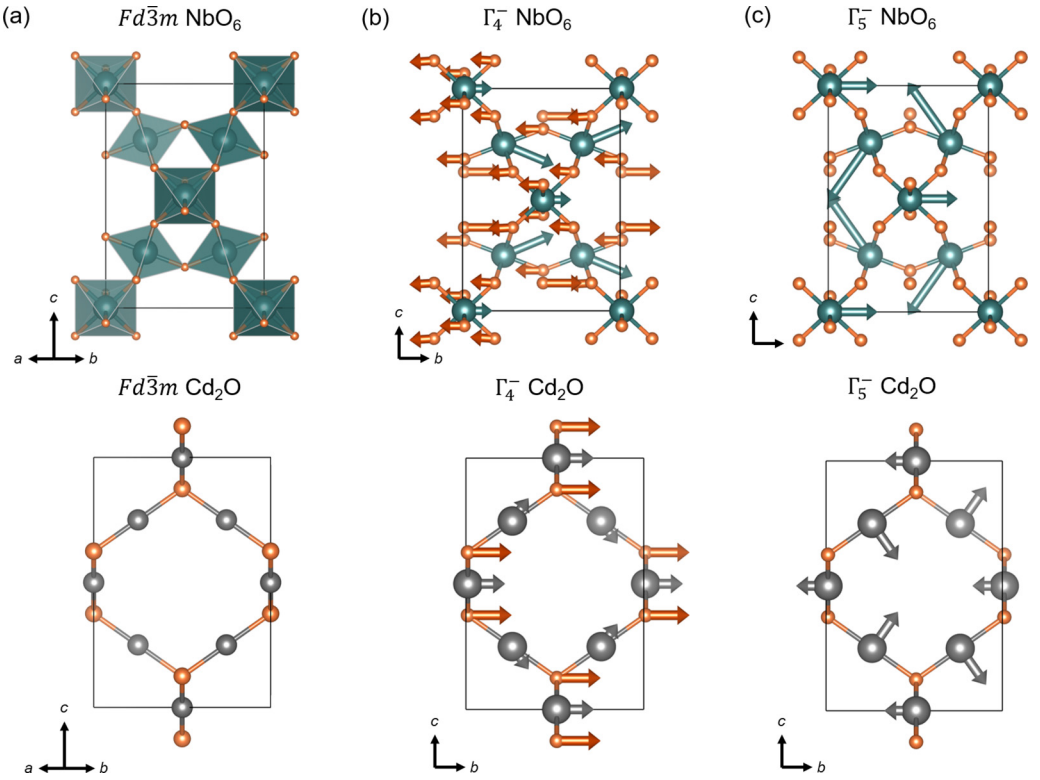

FIG. 1. (a) NbO_6 and Cd_2O sublattice positions in the ideal $Fd\bar{3}m$ structure and subsequent (b) Γ_4^- and (c) Γ_5^- mode distortions that lead to the low-temperature $Ima2$-α polar structure. Adapted from Laurita *et al.* [7].

$Ima2$-α and the Γ_4^--dominant phase suggested by DFT as $Ima2$-β in the remainder of the paper.

At temperatures below 100 K, two further transitions occur to monoclinic phases, with likely space group Cc [9,11]. Refinements to date have not been performed for these two monoclinic phases. Again, DFT studies for the suggested Cc space group indicate that Γ_4^- should be dominant. Moreover, the phase transition picture is further complicated by the presence of several additional strain and displacive modes [6], whose role in the stabilization of the various phases is poorly understood.

In this study, we find from an analysis of x-ray data a local structure that is dominated by Γ_4^-, but reduces to a dominant Γ_5^- for the global structure. This finding is further supported by our DFT study. Such "averaging out" of the polar Γ_4^- distortions over long distances is typical behavior for a relaxor ferroelectric. Intriguingly, some of our local structural descriptions exhibit two-in/two-out behavior of the Nb displacements, as previously suggested by Malcherek based on simulations of diffuse scattering data [12]. Although those data suggest $Cd_2Nb_2O_7$ might be a long-sought charge analog of pyrochlore spin ices [13], our results are more consistent with a Heisenberg-like rather than Ising description of the dipolar fluctuations.

II. METHODS

A. Density functional theory

First-principles calculations were performed using DFT as implemented in the Vienna *ab initio* simulation package (VASP) [14,15] using a plane-wave basis set with a 750-eV energy cutoff. The Perdew–Burke–Ernzerhof (PBE) exchange-correlation functional revised for solids (PBEsol) [16] was employed, along with the projector augmented wave (PAW) potentials to treat the separation of the core and valence electrons [17].

Energy surfaces were generated by perturbing the high-symmetry cubic experimental structure (as refined in Ref. [7]) along the soft eigendisplacements of the force constant matrix. These form two triply degenerate sets of orthogonal displacement vectors (exhibiting Γ_4^- and Γ_5^- symmetry, respectively), with each set of displacements forming a three-dimensional (3D) distortion space. These 3D distortion spaces were studied by perturbing the crystal structure along linear combinations of the basis eigenvectors and then relaxing the primitive cell size and shape until the forces and stress tensor were converged to 2 meV $Å^{-1}$ and 5 meV $Å^{-2}$, respectively.

B. Sample preparation

A polycrystalline sample of $Cd_2Nb_2O_7$ was prepared by mixing a stoichiometric ratio of CdO (Alfa Aesar, 99.998%) and Nb_2O_5 (Alfa Aesar, 99.998%). The sample was pressed into a pellet and fired in air at 500 °C for 10 h to prevent Cd volatilization, followed by a subsequent grinding, pressing, and heating at 1000 °C for 12 h.

C. X-ray scattering

X-ray pair distribution function (XPDF) measurements were performed at the National Synchrotron Light Source II, Brookhaven National Laboratory, on the Pair Distribution

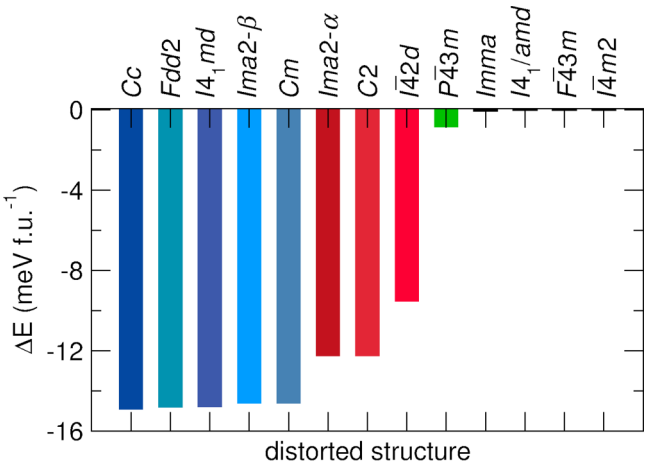

FIG. 2. Calculated energies for $Cd_2Nb_2O_7$ in various space groups relative to the cubic phase. The bars colored in blue have a dominant Γ_4^- component, the ones in red a dominant Γ_5^- component, and the variant in green is driven by an X_4 mode. The four structures on the right without bars are associated with modes that are stable, and therefore do not lower the energy. Updated from Laurita *et al.* [7].

Function (PDF) beamline. The sample was ground into a fine powder and loaded into a 1-mm Kapton capillary for measurement. Data were collected upon cooling with a wavelength of 0.1665 Å every 20 K from 300 K down to 80 K. Two-dimensional (2D) scattering data were collected on a Perkin–Elmer flat-panel amorphous Si-based area detector run at 4 Hz, with each data set corresponding to the sum of 60-s data collection (240 frames). Empty Kapton capillaries were measured under identical conditions and used for background subtraction. GSAS-II [18] was utilized to integrate the two-dimensional (2D) data to one-dimensional (1D) diffraction patterns. Corrections to obtain $S(Q)$ and subsequent Fourier transform with $Q_{max} = 22$ Å^{-1} and an r grid of 0.01 Å were performed using the program PDFGETX3 [19] to obtain the x-ray pair distribution function $G(r)$. These parameters were chosen to optimize the resolution while minimizing Fourier termination ripples satisfactorily for all temperatures across the series. Least-squares refinement of the XPDF data were performed with PDFGUI [20].

III. RESULTS AND DISCUSSION

A. Previous DFT results

An important finding of previous DFT studies is that a number of space groups have almost identical energies (Fig. 2), with the Γ_4^--dominated ones having an energy only a few meV per formula unit below those of the Γ_5^--dominated ones, which are in turn also close in energy [7]. This implies almost isotropic energy surfaces for both modes, which are also coupled to one another. The Landau theory for this has been written out in our previous study [21], where we also illustrated the existence of various Higgs and Goldstone modes, and their antiphase variants (Leggett modes), that should exist as a consequence. The former are also found to play an important role in the related pyrochlore $Cd_2Re_2O_7$ [22,23].

B. Local versus global structure

This brings up the question of the nature of the phase transitions at 204 K and 196 K (it is below the latter temperature that relaxor behavior is most apparent). It has been proposed that in the ferroelectric phase, there is a mixture of order-disorder and displacive behavior, with experimental results indicating that Nb is primarily displacive, whereas Cd is primarily order-disorder [6,12,24]. Alternatively, Γ_5^- may be more displacivelike while Γ_4^- may be more order-disorder-like. This highlights the fact that the DFT analysis is for a homogeneous material, whereas relaxor behavior implies local inhomogeneities.

To address these points, we note that while crystallographic analysis (such as Rietveld refinement) can provide a detailed description of global order and phase transitions as a function of temperature, local probes are necessary to reveal any local distortions or midrange ordering that might average out in a global refinement. Techniques such as IR and Raman spectroscopy are valuable for describing the coordination environment of the cations, but are unable to describe any structural ordering between next-nearest neighbors, such as Cd-Cd/Nb-Nb (M-M) and Cd-Nb (M-M') interactions. The pair distribution function (PDF) is obtained from a combination of Bragg and diffuse scattering events when a material is irradiated, and is a histogram of all atom-atom interactions in a material, presented as a function of r range. This technique is similarly useful for describing coordination environments (typically captured in peaks below 3 Å), and can additionally provide insight on mid- to long-range atomic correlations.

Local ordering is often hidden as structural disorder in the form of enlarged atomic displacement parameters in a Rietveld refinement, but can have a meaningful impact on the observed behavior of a material, such as relaxor behavior. In this study, "local" correlations were fit over a range of 1.7–5.7 Å, "midrange" correlations were fit over a range of 1.7–12.0 Å, and "long-range" or "average" correlations were fit over a range of 5.7–30 Å. For our study, x-ray scattering was chosen as a probe due to the high neutron absorption cross section of Cd (2520 barn) [25]. It should be noted that this necessary choice unfortunately deemphasizes contributions from oxygen, which is a poor scatterer of x-rays in comparison to the heavy metals in $Cd_2Nb_2O_7$; however, meaningful information about Cd-Cd/Nb-Nb (M-M) and Cd-Nb (M-M') interactions can be obtained, as well as some information on Cd-O and Nb-O bond interactions. Data were collected from room temperature to 80 K to elucidate any local behavior in the cubic and orthorhombic phases, and as such our analysis will not experimentally address the lower-temperature monoclinic phases mentioned above.

C. Local Γ_4^- displacements: DFT simulations

Before analyzing the coupling and competition between the two dominant distortion modes, we consider the energy landscape associated with each mode independently. Using the eigendisplacements of the force constant matrix as a basis set, we compute the energy surfaces for pure Γ_4^- and pure Γ_5^- distortions in three dimensions (Fig. 3). Corresponding order-parameter directions and symmetries for the modes are

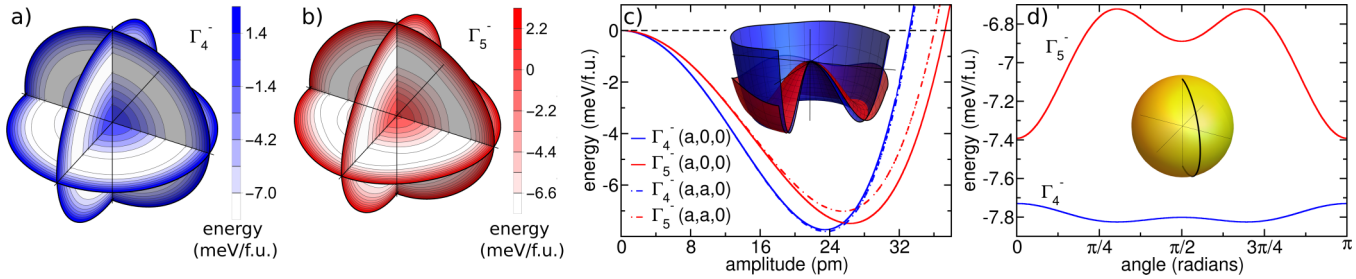

FIG. 3. [(a), (b)] Contour maps of the energy surfaces for the three-dimensional (a) Γ_4^- and (b) Γ_5^- distortion modes. (c) Energy reduction relative to the cubic phase as a function of distortion amplitude along the (a,0,0) (solid curves) and (a,a,0) (dot-dashed curves) order parameter directions for Γ_4^- and Γ_5^-. The inset shows the two-dimensional energy surfaces defined by the order parameter (a,b,0) for Γ_4^- and Γ_5^-. (d) Energy reduction relative to the cubic phase with constant distortion amplitude, r, varying the order parameter direction for Γ_4^- and Γ_5^- through one half of a great circle, that is, (a,a,b) with $2a^2+b^2=r^2$, following the path shown by the black curve on the sphere in the inset.

given in Table I. We find that both energy surfaces are remarkably isotropic, resulting in a 3D version of the well-known "Mexican hat" potential that describes the corresponding 2D case. Pure displacements associated with the order parameter direction along the cubic axes are slightly more energetically favorable than off-axis directions for Γ_5^-, but for the most part a displacement of a given magnitude lowers the energy to the same degree regardless of the order parameter direction [Fig. 3(c)]. The particularly high degree of Γ_4^- isotropy is consistent with polarization measurements near the ferroelectric transition temperature, which found that the polarization direction is easily rotated by an electric field [5]. Note that these calculations describe the 0 K state, and we might expect thermal energy to further reduce the weak anisotropy. Indeed, the barrier between energy minima is less than 0.5 meV/f.u. for Γ_5^- and less than 0.1 meV/f.u. for Γ_4^- [Fig. 3(d)], implying fluctuations between order parameter directions should readily take place. A similar behavior for the energy surface of Γ_4^- has been remarked on for perovskite relaxors [26].

Whereas the energy scales are comparable, we nonetheless observe that the Γ_4^- mode is both more unstable (i.e., it has a more negative curvature of the energy versus displacement around zero amplitude) and has a lower energy minimum than Γ_5^-, consistent with previous first-principles investigations [7,9]. Until now, this has been perceived as inconsistent with experimental measurements, where Γ_5^- displacements dominate the global refinement [6]. However, the isotropic energy surfaces of the two modes imply that long-range characterization techniques may be blind to the local mode dynamics along the energy surfaces [21]. We also observe that the Γ_4^- energy surface is significantly more isotropic than the Γ_5^- one [Figs. 3(c) and 3(d)], implying that the Γ_4^- distortions exhibit a greater degree of disorder at higher temperatures. Conversely, the larger anisotropy of the Γ_5^- energy surface enables Γ_5^- to condense over longer length scales than Γ_4^-, consistent with the dominance of the Γ_5^- mode in global refinements of the crystallographic structure.

TABLE I. Order parameter directions for space groups within the manifold of Γ_4^-, Γ_5^- modes (generated using Ref. [27]).

Γ_4^-	Γ_5^-	Space Group
(a,0,0)		$I4_1md$
	(a,0,0)	$I\bar{4}2d$
(a,0,0)	(0,b,0)	$Fdd2$
(a,a,0)	(0,b,-b)	$Ima2$
(a,b,0)	(0,c,d)	Cc
(a,a,b)	(0,c,-c)	Cm

D. Local Γ_4^- displacements: X-ray scattering

To investigate this further, we performed XPDF measurements as a function of temperature and fit the results with a variety of space groups suggested from the calculated energy surface as possible descriptions of the local symmetry breaking. Eight candidate models with decreasing symmetry/ordering were chosen to fit the data, falling into four categories: (1) the high-temperature cubic $Fd\bar{3}m$ structure, (2) five candidate structures dominated by the Γ_4^- distortion mode, (3) two candidate structures dominated by the Γ_5^- distortion mode, and (4) an orthorhombic $Imma$ structure previously suggested as the intermediate phase between $Fd\bar{3}m$ and $Ima2$ [for categories (2) and (3), see Table I]. All structures were derived from our previous work on $Cd_2Nb_2O_7$ [7], except for the Γ_4^--dominated Cc structure which was taken from Ref. [9] and further relaxed with DFT. To minimize the number of refined parameters in the least-squares analysis of the PDF, atomic positions were fixed to the theoretical atomic positions obtained from the DFT analysis. Due to the minimal x-ray scattering power of oxygen in the presence of heavier cations, the oxygen atomic displacement parameters (ADPs) were modeled as being isotropic (U_{iso}) with a fixed value of 0.01 Å^2. For these fits, the scale, lattice parameters, and isotropic Cd and Nb ADPs were allowed to refine, and a correlated motion correction (δ-2) was applied to the fits to account for peak sharpening at low r. Goodness of fit (reported as R_w) as a function of temperature for each candidate space group is shown in Fig. 4.

From a long-range perspective (correlations up to 30 Å), the space groups dominated by Γ_4^- distortions better fit the data at high temperature, with a crossover to structures dominated by the Γ_5^- distortion mode around 140 K [bottom graph of Fig. 4(a)]. This length scale provides a description of the data closer to the crystallographic structure (i.e., encompass-

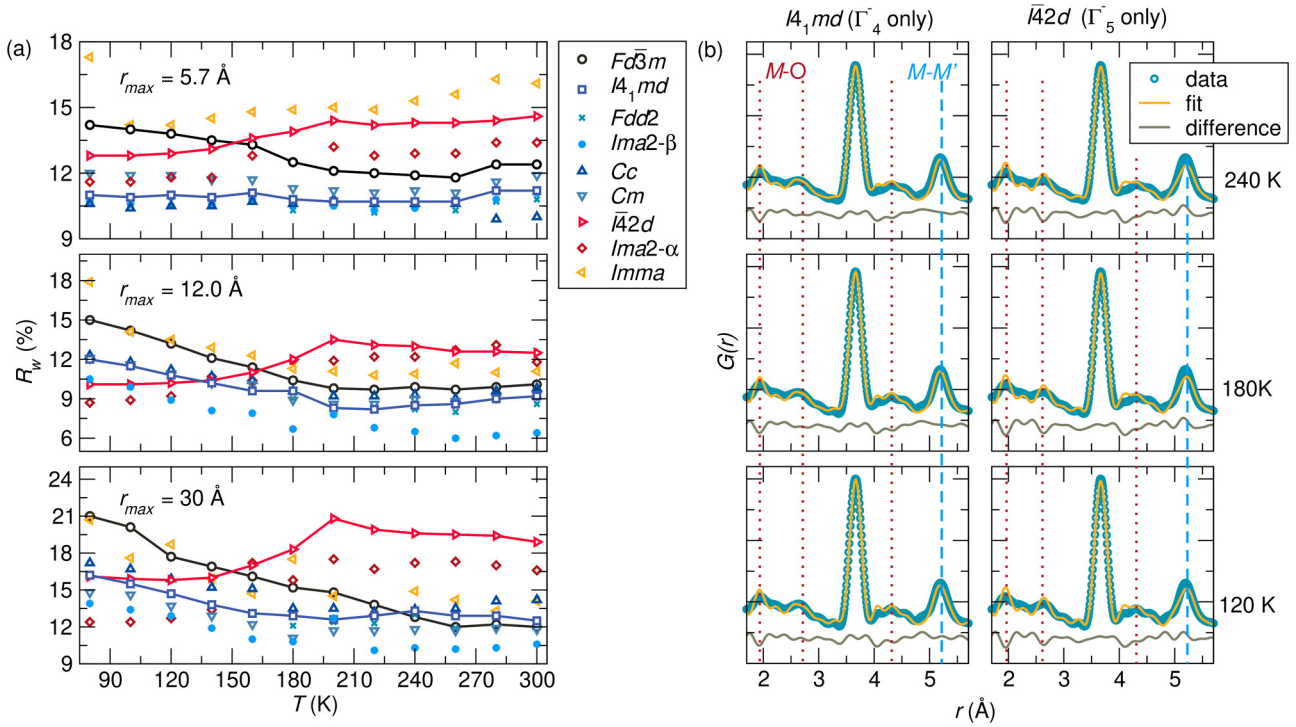

FIG. 4. (a) Goodness of fit (R_w) as a function of temperature for a series of candidate space groups with a fit r_{max} of 5.7 Å, 12.0 Å, and 30 Å. The fit against the cubic $Fd\bar{3}m$ structure is shown as black circles, space groups with primarily Γ_4^- distortion modes are shown as blue symbols, space groups with primarily Γ_5^- distortion modes are shown as red symbols, and the space group with a primary Γ_5^+ distortion mode (*Imma*) is shown as yellow symbols. (b) Local fits (1.7–5.7 Å) of the XPDF data against the $I4_1md$ and $I\bar{4}2d$ space groups at 240 K, 180 K, and 120 K. The *M*-O correlations are indicated by the red short-dash lines and the *M*-*M*′ correlations by the blue long-dash lines.

ing several degrees of atom-atom interactions), but does not capture any microstructural effects that might be at play, such as the role of nanodomains in the material. Such analysis would be better suited to microscopy studies [28], which are outside the scope of the present work.

It should be noted that, whereas the XPDF fits provide insight into the prevalence of Γ_4^- versus Γ_5^--type local distortion patterns, it is important to be conservative in stating which specific structure is the best description. For instance, the *Cm* space group has nine refined parameters as opposed to three in $Fd\bar{3}m$, five in $Fdd2$, seven in $Ima2$, and eight in Cc. Nonetheless, since all Γ_4^--based structures have a lower R_w than both of the Γ_5^- space groups, we can say that the Γ_4^- distortion pattern better describes the data over this fit range.

At 300 K, both cubic and Γ_4^--type models equally describe the data out to 30 Å, with the highest symmetry cubic $Fd\bar{3}m$ having larger atomic displacement parameters (ADPs) and the lowest symmetry *Cm* structure having small distortions in the atomic positions, suggesting that the cubic and Γ_4^--type models are equivalent descriptions at this length scale. However, both the enlarged anisotropic ADPs in the ideal $Fd\bar{3}m$ model and atom off-centering in the Γ_4^- models indicate that distortions are present and cations are not located at the center of their coordination environments. In the midrange region [correlations up to 12 Å, middle graph of Fig. 4(a)], the trend is similar to the long-range fits, with $Ima2$-β providing a better description of the midrange structure upon cooling to 120 K, whereas $Ima2$-α becomes the better description of correlations at this length scale for lower temperatures. In the local range [correlations up to 5.7 Å, top graph of Fig. 4(a)], the space groups with primarily Γ_4^- distortion modes provide a better fit of the data at all temperatures. *Cc* has the lowest R_w at 300 K and exhibits similar R_w values to *Cm*, $Ima2$-β, and $Fdd2$ upon cooling.

To better understand the nature of the distortions, comparisons of the fits to the $I4_1md$ (Γ_4^- only) and $I\bar{4}2d$ (Γ_5^- only) structures above (240 K), near (180 K), and below (120 K) the ferroelectric transition were performed. The local fits (1.7–5.7 Å) to the XPDF are shown in Fig. 4(b). At all temperatures, $I4_1md$ provides a better fit than $I\bar{4}2d$ of the Cd-O peaks (Cd coordination environment) and the *M*-*M*′ peak at approximately 5.2 Å, which is the next-nearest Cd-Nb correlation. Moreover, at all temperatures, $Fdd2$ further improves the fit of all *M*-O peaks. $Ima2$-β has a similar improvement in the *M*-O local peaks, in addition to a better fit of the midrange *M*-*M* and *M*-*M*′ peaks. This is illustrated for 300 K data in Fig. 5.

E. Intermediate phase scenario

Neither our first-principles results nor our experimental data provide strong evidence of an intermediate phase between 204 K and 196 K belonging to point group *mmm* before the relaxor ferroelectric transition occurs. We calculate no unstable or low-lying phonon modes in the high-symmetry structure which break the requisite symmetries, and XPDF data do not favor the *Imma* structure at any length scale. Based on the above results, we can offer a possible scenario for the

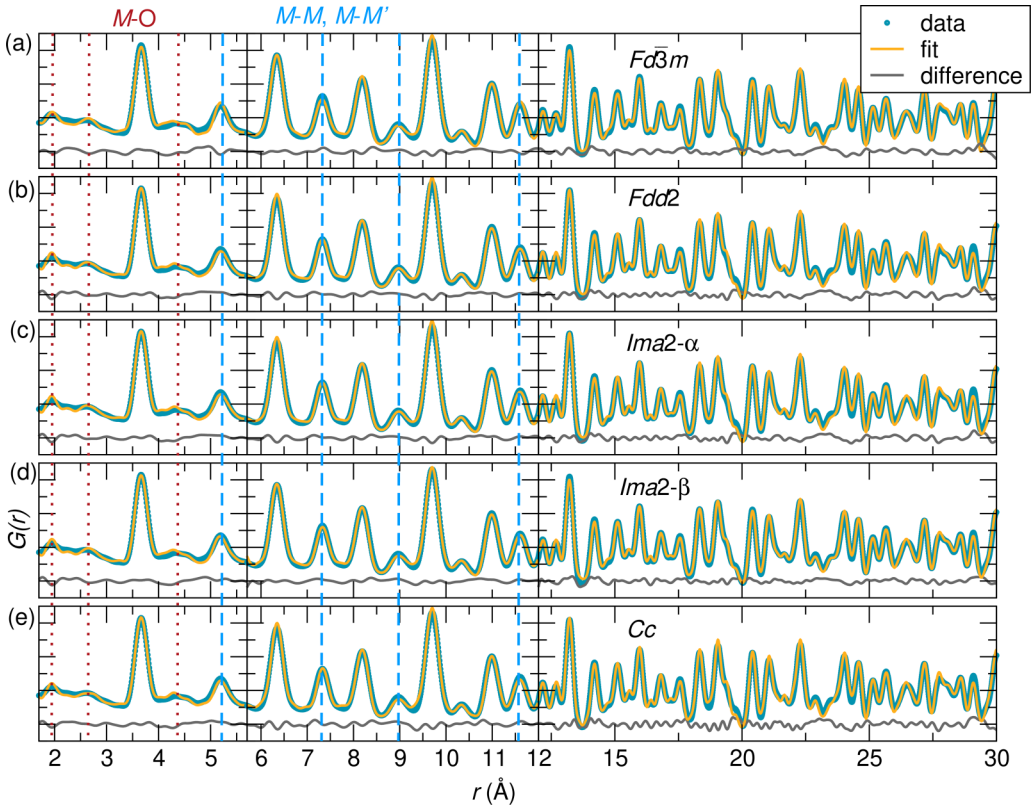

FIG. 5. Fits of the XPDF data collected at 300 K against proposed structures for $Cd_2Nb_2O_7$: (a) cubic $Fd\bar{3}m$, (b) orthorhombic $Fdd2$, (c) orthorhombic $Ima2$-α, (d) orthorhombic $Ima2$-β, and (e) monoclinic Cc. Fit ranges are indicated by the range shown in each panel, M-O correlations of interest are shown as short red dashes, and M-M/M-M' correlations of interest are shown as long blue dashes.

intermediate phase. Our DFT results indicate that Cm, Cc, $Ima2$-β, $Fdd2$, and $I4_1md$ structures have almost identical energies (Fig. 2). The last two only differ in that $I4_1md$ has no Γ_5^- component. To understand the proposed scenario, note that $Fdd2$, $Ima2$, and Cc define a great circle on each of the Γ_4^- and Γ_5^- energy surfaces (Γ_4^- and Γ_5^- are each three-dimensional irreps, see Fig. 3), with $Fdd2$ corresponding to $\phi = 0°$, $Ima2$ to $\phi = 45°$, and Cc to an intermediate angle, as can be seen from Table I [21]. This is exactly analogous to $Cd_2Re_2O_7$, where the respective space groups are $Ima2$, $I4_122$, and $F222$. For the latter, one has a proposed sequence of transitions from $Fd\bar{3}m \rightarrow I4m2 \rightarrow I4_122 \rightarrow F222$ [29], which corresponds to various positions around the brim of the "Mexican hat" energy surface (in this case, from Γ_3^-, which is a two-dimensional irrep). The analogous series for $Cd_2Nb_2O_7$ would be $Fd\bar{3}m \rightarrow Fdd2 \rightarrow Ima2 \rightarrow Cc$. There are several points in favor of this scenario, in that it explains the experimental absence of the (0,0,10) Bragg peak in the temperature range of 196 K–204 K [8], since this is allowed for $Ima2$ but not for $Fdd2$. It also explains why optical studies indicate a ferroelectric polarization vector along the cubic axis [5] as opposed to $Ima2$ where it is along (1,1,0) instead. $Fdd2$ is also found to be the global space group upon sulfur doping [7] and has been proposed to be the local structure for $Cd_2Nb_2O_7$ itself [12]. The claim of a centrosymmetric space group (mmm point group) in this temperature range [5] could then be a domain averaging effect, similar to the phenomenon observed in cubic $BaTiO_3$ [30].

F. Cd and Nb displacements

Our results help to explain the challenges associated with identifying possible intermediate space groups. The isotropic energy surfaces (Fig. 3) imply that local distortions along multiple order parameter directions may occur simultaneously, a result corroborated by the number of space groups with comparable goodness of fit in the XPDF data. The observation that local fits differ significantly from the mid- and long-range fits also supports the conclusion that local structural disorder (in the form of uncorrelated atomic displacements) plays a large role in the relaxor ferroelectric transition of $Cd_2Nb_2O_7$.

The combination of DFT and our XPDF data implies a distinction between the role of the two primary distortion modes. Γ_4^- displacements dominate the local structure even at high temperatures, whereas Γ_5^- displacements condense over longer length scales at lower temperatures, consistent with previous global refinements [6].

Visualizing the Γ_4^- and Γ_5^- displacement patterns (Fig. 6) also allows us to comment on the relative role of Cd and Nb in the phase transitions. As Nb displacements (likely due to the second-order Jahn–Teller effect typical of d^0 ions) are central to the ferroelectric behavior, we turn to a detailed description of these. As commented on by Malcherek [12], $Fdd2$ is a possible description of the local structure. This is not inconsistent with our analysis, in that $Fdd2$ produces one of the lowest R_w values at the local scale below 270 K [Fig. 4(a)] and corresponds to a local energy minimum for the Γ_4^- mode (see Table I and Fig. 3). The $Fdd2$ displacements

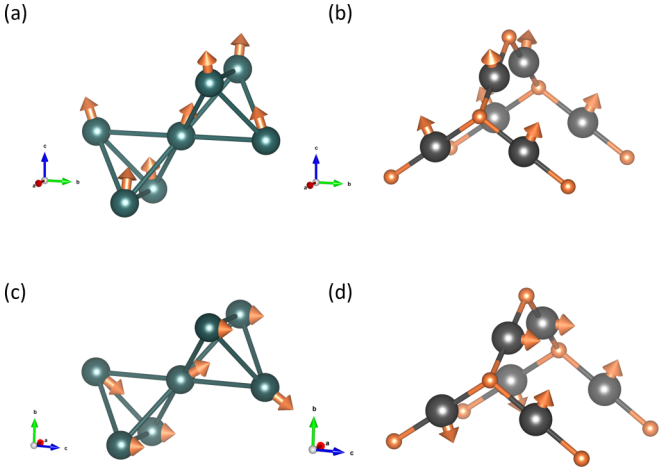

FIG. 6. [(a), (b)] Displacement pattern of the relaxed $Fdd2$ structure relative to the high-symmetry cubic structure ($Fd\bar{3}m$) for the (a) Nb sublattice and (b) Cd-O sublattice. [(c), (d)] Displacement pattern of the relaxed Γ_4^--dominated $Ima2$-β structure relative to the high-symmetry cubic structure ($Fd\bar{3}m$) for the (c) Nb sublattice and (d) Cd-O sublattice.

correspond to the classic two-in/two-out behavior characteristic of spin moments in pyrochlore spin ices. That is, for a given tetrahedron of Nb, two of the Nb displacements point inwards, two point outwards (Fig. 6), with the Nb displacements along the Nb-Nb bond directions as opposed to along the local trigonal axis as in spin ices (here, the polar displacement along c drops out, since all Nb ions are shifted by this). A similar picture has been advocated for Bi displacements in $Bi_2Ti_2O_7$ [13]. This implies that some of the same physics found in spin ices might be relevant for the dielectric response for $Cd_2Nb_2O_7$. In particular, violation of the ice rules leads to the creation of monopole-antimonopole pairs (i.e., three-in/one-out–three-out/one-in), whose dynamics can explain the Vogel–Fulcher relation for the relaxation rate. We note that monopole-antimonopole pairs have also been invoked in the context of cubic perovskite relaxors, where they represent eight-in–eight-out instead [31].

However, as noted above, assignment of a specific local space group on the basis of our XPDF data is inadvisable. For example, XPDF fits against $Ima2$-β (Γ_4^--dominated) can produce R_w values even lower than $Fdd2$. This can be attributed in part to the larger number of structural parameters in $Ima2$-β than $Fdd2$, but nevertheless we cannot justify ascribing the local structure to one or the other. Similarly, the energy difference between $Fdd2$ and $Ima2$-β as computed with DFT is below 1 meV/f.u., meaning neither can be called more energetically favorable. Therefore, while a charge ice description of $Cd_2Nb_2O_7$ is attractive, our results indicate a more Heisenberg-like description of the dipolar fluctuations than the Ising-like one implied by a charge ice picture. That is, our data depict an isotropic, Γ_4^--dominated energy surface (Fig. 3), implying that Nb atoms displace within their local coordination environments along various order parameter directions within the Γ_4^- distortion space.

We now turn to Cd displacements. Cd has two short bonds with oxygen along its local trigonal axis [O(2) ions] and six long bonds with oxygen in the NbO_6 octahedra [O(1) ions]. To improve bonding with the O(1) ions, Cd displaces normal to the local trigonal axis (Fig. 6), as is seen in many pyrochlores. For instance, diffuse scattering in $La_2Zr_2O_7$ finds a pronounced annular displacement of La normal to the local trigonal axis [32], consistent with what we find for Cd in $Cd_2Nb_2O_7$, and Cd likely remains disordered in the ferroelectric phase [24]. As such, Cd displacements are unlikely to drive the symmetry lowering either locally or over longer ranges.

IV. CONCLUSION

We have presented evidence that $Cd_2Nb_2O_7$ is locally characterized by the ferroelectric mode Γ_4^- but globally described by the nonpolar mode Γ_5^-. This observation relates this pyrochlore to perovskite relaxor ferroelectrics whose relaxor behavior is attributed to local polar clusters [1]. Recently, further insights into relaxor behavior in perovskites have been achieved by contrasting XPDF, which emphasizes higher Z ions, with neutron PDF where oxygens play a significant role [33]. A neutron PDF analysis in $Cd_2Nb_2O_7$ would be possible with Cd isotopically enriched samples. This could be complemented by a DFT determination of the various parameters in the Landau free energy that has been critical in studies of structural phase transitions, such as in the perovskite $YMnO_3$ where the amplitude of the structural order parameter is order-disorder-like but the phase behaves displacively [34–36], a study we hope to report on in the future.

In addition, we have presented candidate descriptions of the local structure, some of which ($Fdd2$ and $I4_1md$) are dominated by two-in/two-out displacements of Nb ions in a given Nb tetrahedron, which might imply that $Cd_2Nb_2O_7$ is a charge ice analog of the pyrochlore spin ices that have been much studied in the past two decades. Our results, however, are consistent with a richer energy landscape that is more Heisenberg-like than Ising-like. Therefore, inspired by recent work in spin ices [2–4], we believe that the dynamics of the dielectric response of $Cd_2Nb_2O_7$ is worth reinvestigating.

ACKNOWLEDGMENTS

D.H.Y. and J.M.R. were supported by the National Science Foundation (NSF) under Award No. DMR-2011208. G.L. acknowledges support for this work from Bates College, and from the National Science Foundation (NSF) through Award No. DMR-1904980. M.R.N. was supported by the Materials Sciences and Engineering Division, Basic Energy Sciences, Office of Science, U.S. Department of Energy. N.A.S. was supported by the European Research Council (ERC) under the European Unions Horizon 2020 Research and Innovation Program project HERO (Grant No. 810451) and by ETH Zurich. Q.N.M. was supported by the Swiss National Science Foundation under Project No. P2EZP2_191872. This research used the Pair Distribution Function (PDF) beamline of the National Synchrotron Light Source II, a U.S. Department of Energy (DOE) Office of Science User Facility operated for the DOE Office of Science by Brookhaven National Laboratory under Contract No. DE-SC0012704. Calculations were performed using the Department of Defense High Performance Computing Modernization Program (DOD-HPCMP).

[1] R. A. Cowley, S. N. Gvasaliya, S. G. Lushnikov, B. Roessli, and G. M. Rotaru, Relaxing with relaxors: A review of relaxor ferroelectrics, Adv. Phys. **60**, 229 (2011).

[2] E. R. Kassner, A. B. Eyvazov, B. Pichler, T. J. S. Munsie, H. A. Dabkowska, G. M. Luke, and J. C. Seamus Davis, Supercooled spin liquid state in the frustrated pyrochlore $Dy_2Ti_2O_7$, Proc. Natl. Acad. Sci. **112**, 8549 (2015).

[3] A. B. Eyvazov, R. Dusad, T. J. S. Munsie, H. A. Dabkowska, G. M. Luke, E. R. Kassner, J. C. S. Davis, and A. Eyal, Common glass-forming spin-liquid state in the pyrochlore magnets $Dy_2Ti_2O_7$ and $Ho_2Ti_2O_7$, Phys. Rev. B **98**, 214430 (2018).

[4] A. M. Samarakoon, A. Sokolowski, B. Klemke, R. Feyerherm, M. Meissner, R. A. Borzi, F. Ye, Q. Zhang, Z. Dun, H. Zhou, T. Egami, L. Jaubert, C. Castelnovo, R. Moessner, S. A. Grigera, and D. A. Tennant, Structural magnetic glassiness in spin ice $Dy_2Ti_2O_7$, Phys. Rev. Research **4**, 033159 (2022).

[5] Z. G. Ye, N. N. Kolpakova, J.-P. Rivera, and H. Schmid, Optical and electric investigations of the phase transitions in pyrochlore $Cd_2Nb_2O_7$, Ferroelectrics **124**, 275 (1991).

[6] T. Malcherek, U. Bismayer, and C. Paulmann, The crystal structure of $Cd_2Nb_2O_7$: Symmetry mode analysis of the ferroelectric phase, J. Phys.: Condens. Matter **22**, 205401 (2010).

[7] G. Laurita, D. Hickox-Young, S. Husremovic, J. Li, A. W. Sleight, R. Macaluso, J. M. Rondinelli, and M. A. Subramanian, Covalency-driven structural evolution in the polar pyrochlore series $Cd_2Nb_2O_{7-x}S_x$, Chem. Mater. **31**, 7626 (2019).

[8] M. Tachibana, K. Fritsch, and B. D. Gaulin, X-ray scattering studies of structural phase transitions in pyrochlore $Cd_2Nb_2O_7$, J. Phys.: Condens. Matter **25**, 435902 (2013).

[9] M. Fischer, T. Malcherek, U. Bismayer, P. Blaha, and K. Schwarz, Structure and stability of $Cd_2Nb_2O_7$ and $Cd_2Ta_2O_7$ explored by *ab initio* calculations, Phys. Rev. B **78**, 014108 (2008).

[10] E. Buixaderas, S. Kamba, J. Petzelt, M. Savinov, and N. Kolpakova, Phase transitions sequence in pyrochlore $Cd_2Nb_2O_7$ studied by IR reflectivity, Eur. Phys. J. B **19**, 9 (2001).

[11] A. Küster, J. Ihringer, W. Limper, T. Wroblewski, and W. Prandl, Symmetry of the ferroelectric phases of the pyrochlore $Cd_2Nb_2O_7$ - A study using a very high resolution powder diffractometer at a synchrotron radiation source, Mater. Sci. Forum **79-82**, 791 (1991).

[12] T. Malcherek, The ferroelectric properties of $Cd_2Nb_2O_7$: A Monte Carlo simulation study, J. Appl. Crystallogr. **44**, 585 (2011).

[13] R. Seshadri, Lone pairs in insulating pyrochlores: Ice rules and high-k behavior, Solid State Sci. **8**, 259 (2006).

[14] G. Kresse and J. Furthmuller, Efficient Iterative Schemes for Ab Initio Total-Energy Calculations using a Plane-Wave Basis Set, Phys. Rev. B **54**, 11169 (1996).

[15] G. Kresse and D. Joubert, From ultrasoft pseudopotentials to the projector augmented-wave method, Phys. Rev. B **59**, 1758 (1999).

[16] J. P. Perdew, A. Ruzsinszky, G. I. Csonka, O. A. Vydrov, G. E. Scuseria, L. A. Constantin, X. Zhou, and K. Burke, Generalized Gradient Approximation for Solids and their Surfaces, Phys. Rev. Lett. **100**, 136406 (2008).

[17] P. E. Blochl, Projector augmented-wave method, Phys. Rev. B **50**, 17953 (1994).

[18] B. H. Toby and R. B. Von Dreele, *GSAS-II*: The genesis of a modern open-source all purpose crystallography software package, J. Appl. Crystallogr. **46**, 544 (2013).

[19] P. Juhás, T. Davis, C. L. Farrow, and S. J. L. Billinge, *PDFgetX3*: A rapid and highly automatable program for processing powder diffraction data into total scattering pair distribution functions, J. Appl. Crystallogr. **46**, 560 (2013).

[20] C. L. Farrow, P. Juhas, J. W. Liu, D. Bryndin, E. Bozin, E. S. J. Bloch, T. Proffen, and S. J. L. Billinge, PDFfit2 and PDFgui: Computer programs for studying nanostructure in crystals, J. Phys.: Condens. Matter **19**, 335219 (2007).

[21] Q. N. Meier, D. Hickox-Young, G. Laurita, N. A. Spaldin, J. M. Rondinelli, and M. R. Norman, Leggett Modes Accompanying Crystallographic Phase Transitions, Phys. Rev. X **12**, 011024 (2022).

[22] C. A. Kendziora, I. A. Sergienko, R. Jin, J. He, V. Keppens, B. C. Sales, and D. Mandrus, Goldstone-Mode Phonon Dynamics in the Pyrochlore $Cd_2Re_2O_7$, Phys. Rev. Lett. **95**, 125503 (2005).

[23] J. Venderley, K. Mallayya, M. Matty, M. Krogstad, J. Ruff, G. Pleiss, V. Kishore, D. Mandrus, D. Phelan, L. Poudel, A. G. Wilson, K. Weinberger, P. Upreti, M. Norman, S. Rosenkranz, R. Osborn, and E.-A. Kim, Harnessing interpretable and unsupervised machine learning to address big data from modern x-ray diffraction, Proc. Natl. Acad. Sci. **119**, e2109665119 (2022).

[24] M. Paściak, M. Wołcyrz, A. Pietraszko, and S. Leoni, Local structure in the paraelectric phase of $Cd_2Nb_2O_7$ determined from x-ray diffuse scattering, by means of *ab initio* molecular dynamics and Monte Carlo modeling, Phys. Rev. B **81**, 014107 (2010).

[25] V. F. Sears, Neutron scattering lengths and cross sections, Neutron News **3**, 26 (1992).

[26] A. A. Heitmann and G. A. Rossetti, Thermodynamics of ferroelectric solid solutions with morphotropic phase boundaries, J. Am. Ceram. Soc. **97**, 1661 (2014).

[27] H. T. Stokes, D. M. Hatch, and B. J. Campbell, ISOTROPY Software Suite.

[28] S. Salmani-Rezaie, K. Ahadi, and S. Stemmer, Polar nanodomains in a ferroelectric superconductor, Nano Lett. **20**, 6542 (2020).

[29] K. J. Kapcia, M. Reedyk, M. Hajialamdari, A. Ptok, P. Piekarz, A. Schulz, F. S. Razavi, R. K. Kremer, and A. M. Oles, Discovery of a low-temperature orthorhombic phase of the $Cd_2Re_2O_7$ superconductor, Phys. Rev. Research **2**, 033108 (2020).

[30] K. Tsuda and M. Tanaka, Direct observation of the symmetry breaking of the nanometer-scale local structure in the paraelectric cubic phase of $BaTiO_3$ using convergent-beam electron diffraction, Appl. Phys. Express **9**, 071501 (2016).

[31] Y. Nahas, S. Prokhorenko, I. Kornev, and L. Bellaiche, Topological Point Defects in Relaxor Ferroelectrics, Phys. Rev. Lett. **116**, 127601 (2016).

[32] Y. Tabira, R. L. Withers, T. Yamada, and N. Ishizawa, Annular dynamical disorder of the rare earth ions in a $La_2Zr_2O_7$ pyrochlore via single crystal synchrotron x-ray diffraction, Z. Kristallogr. **216**, 92 (2001).

[33] M. J. Krogstad, P. M. Gehring, S. Rosenkranz, R. Osborn, F. Ye, Y. Liu, J. P. C. Ruff, W. Chen, J. M. Wozniak, H. Luo, O. Chmaissem, Z.-G. Ye, and D. Phelan, The relation of local order

to material properties in relaxor ferroelectrics, Nat. Mater. **17**, 718 (2018).

[34] S. Artyukhin, K. T. Delaney, N. A. Spaldin, and M. Mostovoy, Landau theory of topological defects in multiferroic hexagonal manganites, Nat. Mater. **13**, 42 (2014).

[35] S. H. Skjærvø, Q. N. Meier, M. Feygenson, N. A. Spaldin, S. J. L. Billinge, E. S. Bozin, and S. M. Selbach, Unconventional Continuous Structural Disorder at the Order-Disorder Phase Transition in the Hexagonal Manganites, Phys. Rev. X **9**, 031001 (2019).

[36] Q. N. Meier, A. Stucky, J. Teyssier, S. M. Griffin, D. van der Marel, and N. A. Spaldin, Manifestation of structural Higgs and Goldstone modes in the hexagonal manganites, Phys. Rev. B **102**, 014102 (2020).